2023 IEEE International Conference on Robotics and Automation (ICRA 2023)
May 29 - June 2, 2023. London, UK

Global Localization in Repetitive and Ambiguous Environments

Zhenyu Wu*, Wei Wang*, Jun Zhang, Qiyang Lyu, Haoyuan Zhang, and Danwei Wang, *Fellow, IEEE*

***Abstract*— Accurate global localization is an essential ingredient for autonomous mobile robots (AMRs) operating in enclosed or partially enclosed repetitive environments (*e.g.,* office corridors, industrial warehouses, transportation centers). In such environments, the Global Navigation Satellite System (GNSS) signals are unreliable or severely degraded. The highly ambiguous structures in such challenging scenarios would also lead the ordinary geometric feature-based LiDAR/visual localization methods to fail. The ambient magnetic field (MF) has exhibited high distinctiveness at different location, which makes it a viable alternative for infrastructure-free AMR localization. However, few of the previous research has been focused on the orientation-dependency and similar-sequential-route limitations of MF-based localization. Thus, this paper proposes a novel probabilistic global localization system with 2-D LiDAR and rotation-invariant magnetic field for AMRs operating in challenging repetitive and ambiguous environments. The proposed localization system mainly consists of: 1) Two-step Initialization: laser distance and MF sequence based matching, and 2) MF-based Pose Tracking: recursive multi-dimensional MF sequence based matching. Extensive experimental results demonstrate the advantageous localization performances of the proposed localization system over the existing methods.**

I. Introduction

Global localization, namely, finding the location and orientation at any starting position, is a critical pre-requisite [1]–[11] for autonomous mobile robots (AMRs) or intelligent vehicles to accomplish tasks such as mapping [12]–[14], place recognition [15]–[18], navigation [19], [20], and collaboration [21], [22]. However, AMR global localization in enclosed or partially enclosed repetitive environments (*e.g.* corridors/aisles, industrial warehouses, transportation centers) still remains challenging and intractable due to perceptual aliasing and ambiguous geometric features [2], [3], [6], [23]. Seldom previous work has been focused on the global localization issue in such scenarios [2], [3], [6], [24]. As we analyzed in our earlier research [2], [6], most of the existing localization solutions in such environments are either highly dependent on the pre-installed infrastructures (*e.g.* WiFi routers, RFIDs), which are inflexible and costly; or rely on the onboard sensors to detect geometric features, which would lead to mis-localization to wrong places and result in drastically degraded performances [3], [23].

One infrastructure-free approach to address this problem is to utilize the ambient magnetic field (MF)-based localization systems [1], [6], [23], [25]–[29]. The ambient MF in the environment comprises the omnipresent geomagnetic field and the MF distortions caused by ferromagnetic objects (*i.e.,* the local anomalies) [25], [28], where the local MF distortions form re-identifiable features in each 3-D MF vector [25] thus making the MF-based system a viable alternative for localization [6], [23]–[34] and navigation [19], [35]. Despite the recent popularity of ambient MF-based localization research in the robotics community [6], [19], [23]–[25], [27], [30]–[33], [36], we found that few of the

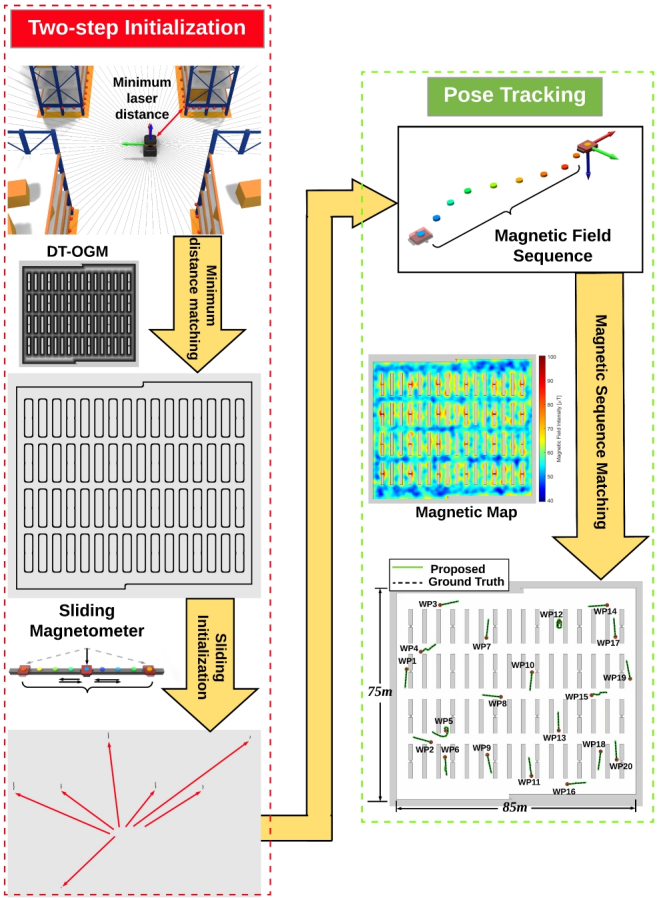

Fig. 1. Demonstrations of the proposed global localization system in simulated industrial warehouse environment. The parts in red dotted box on the left side show the two-step initialization process, where we match the minimum laser distance against the pre-built distance transformed occupancy grid map (DT-OGM), and match the magnetic sequence collected by the sliding magnetometer mechanism against the pre-built magnetic map. The parts in green dotted box on the right side show the process of pose tracking, where magnetic sequences collected after the AMR moves are matched against the magnetic map. In the final results, it is clear that the proposed system can achieve close to ground-truth localization performances in twenty randomly-selected global localization waypoints (WPs).

This research was supported in part by the National Research Foundation, Singapore under its Medium Sized Centre for Advanced Robotics Technology Innovation (CARTIN).

All authors are with the School of Electrical and Electronic Engineering, Nanyang Technological University, Singapore 639798. E-mail: {zhenyu002, wei013}@e.ntu.edu.sg
*Co-first authorship and corresponding author

attention has been paid to the orientation-dependency and similar-sequential-route limitations of the MF [6], [28], [33], [36]. The 3-D MF vector measured by a magnetometer at one single location is highly dependent on the orientation of magnetometer (*i.e.,* orientation-dependency), which is highly sensitive to rotation errors thus causing a strong limitation that hindered the adoption of 3-D MF vector for MF-based localization [28]. Moreover, another important limitation of the MF sequence based matching is the similar-sequential-route [33], [36], which means the online localization MF sequence must have a similar shape with the MF sequence stored in the magnetic map. This may not always be the case in the real-world applications (*e.g.,* the AMR is moving straightly when building the magnetic map, while the AMR is moving in a curved route when doing the localization).

Our earlier research [2] overviewed the challenges of infrastructure-free global localization in repetitive environments and did preliminary tests of several localization methods. Moreover, our previous work [6] explored the feasibility of utilizing the MF to acquire the AMR initial pose and then implementing the 2D LiDAR based algorithm to accurately localize the AMR in repetitive environments. However, there exist ambiguous MF matchings for the single MF fingerprint based initialization and the orientation-dependency limitation of 3-D MF remains unsolved. Inspired by these two work [2], [6], we move one step forward in this paper by proposing a novel probabilistic global localization system with 2-D LiDAR and rotation-invariant MF for AMRs operating in repetitive and ambiguous environments. A concise workflow of the proposed system is shown in Fig. 1. We summarize the main contributions of this paper as follows:

- A novel probabilistic global localization system is proposed, which solves both the orientation-dependency and similar-sequential-route limitations of the MF based localization.
- A sliding magnetometer mechanism onboard the AMR is designed and implemented, which can greatly improve the initialization accuracy and efficiency.
- The practical utility and accuracy of the proposed localization system are extensively verified in both simulated and real-world challenging repetitive experiments.

The rest of this paper is organized as follows. Section II gives a detailed analysis of the rotation-invariant MF characteristics. Section III presents the proposed global localization system. Section IV details the simulations and experimental validations. Section V concludes this paper.

II. Rotation-invariant Magnetic Field

A. Magnetic Field Characteristics

In general, the ambient MF $\mathbf{B}_e \in \mathbb{R}^3$ at the same location can be modeled as a 3-D vector $\mathbf{B}_e = [B_e^x, B_e^y, B_e^z]^T$ within the global coordinate system (*GCS*), where the orthogonal components B_e^x, B_e^y, and B_e^z represent intensities recorded in microtesla (μT) in Geographic North, Geographic East and vertical downward directions (*i.e., NED* coordinate system), respectively. The MF integrated intensity can be represented

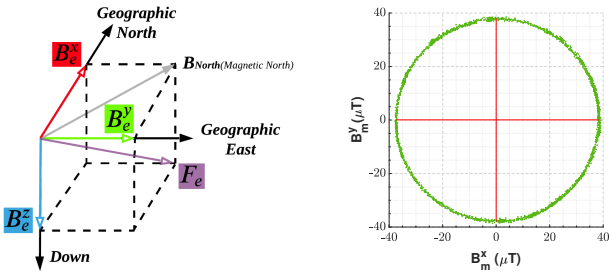

(a) Ambient magnetic field (b) MF with different orientation

Fig. 2. (a) Demonstrations of ambient MF in the *GCS*. If without strong magnetic distortions, the vector sum of B_e^x and B_e^y will point at the direction of *Magnetic North* B_{North} (shown as grey line); (b) Demonstrations of measured MF data in the x/y-axes B_m^x and B_m^y with different orientations at the same location, where the shape is close to a circle with same radius that indicates a stable horizontal component B_m^h.

as $F_e = \sqrt{(B_e^x)^2 + (B_e^y)^2 + (B_e^z)^2}$, which is demonstrated in Fig. 2a. The ambient MF measured in the sensor/local coordinate system (*LCS*) is dependent on the orientation of the magnetometer, which can be defined as [28]:

$$\mathbf{B}_m = W\, R_z(\gamma) R_y(\theta) R_x(\phi) \mathbf{B}_e + V \tag{1}$$

where $\mathbf{B}_m$ denotes the calibrated MF measurements. $R_z(\gamma), R_y(\theta), R_x(\phi)$ are the corresponding rotation matrices in yaw (azimuth), pitch, and roll, respectively. W and V are the soft-iron effect matrix and hard-iron effect offset vector of the magnetometer itself, respectively. Due to the influence of noise, the locus of the measured MF data will be an ellipsoid, where it will be similar to a sphere if the magnetometer is well-calibrated. Before usage, we follow the standard rotation-based process to calibrate the magnetometer [37].

In order to show the orientation-dependent characteristic of the ambient MF, we collect the ambient MF data at the same location in an environment but with different orientations of the magnetometer, where the results are shown in Fig. 2b. It can be observed that the MF data collected at different orientations exhibits dramatic variations in the x/y-axes, while the MF horizontal component B_m^h (*i.e.*, radius of the circle) remains stable. However, solely utilizing the 1-D MF intensity for localization tasks would greatly decrease its discernibility. Existing solutions for this orientation-dependency problem including the assumption of AMR orientation consistency between offline mapping and online localization [2], [6], [27], or fusing with other infrastructure-based methods [31], where both of them did not essentially solve this limitation. Thus, we propose the rotation-invariant MF vector to address this problem.

B. The Rotation-invariant Magnetic Field Vector

Due to the aforementioned MF orientation-dependent characteristic, the direct usage of 3-D MF vectors is a challenging and intractable problem. This means that only after the heading direction is determined, the measured MF in a magnetometer's *LCS* can be generalized to describe a vector measurement. However in practical tasks, the IMU

mounted on the AMR can head towards any direction with the yaw angle $\psi \in [0, 2\pi)$ where the 0 radian is defined with respect to the direction of *Magnetic North*.

Therefore, we present a novel rotation-invariant augmentation of the MF vector in this paper. The proposed MF vector comprises the horizontal component, vertical component, and intensity of the measured MF. The online MF data $\mathbf{B}_m$ is measured in the *LCS* and can be aligned in the unified *GCS* as aforementioned in Section II-A. We define the measured MF data as $\mathbf{B}_m = [B_m^x, B_m^y, B_m^z, F_m]^T$. We focus on the 3-DoF localization problem, thus the rotation matrices in pitch and roll are both set to identity matrix. Eventually, the transformed rotation-invariant MF vector $\mathbf{B}_m^e$ in the *GCS* can be written as:

$$\mathbf{B}_m^e = [B_m^h, B_m^v, F_m]^T = R_z^\top(\psi)\mathbf{B}_m \tag{2}$$

where ψ is the yaw angle of the AMR, the rotation-invariant horizontal component $B_m^h = \sqrt{(B_m^x)^2 + (B_m^y)^2}$ is orthogonal to the vertical component B_m^v, and the vertical component $B_m^v = B_m^z$ is in parallel direction with the unit vector n of the Earth gravity field. The MF vector defined in the *GCS* should be static when the AMR rotates but without any translational movement.

III. The Proposed Probabilistic Global Localization System

In this section, the proposed probabilistic global localization system is analyzed in detail. The framework of the proposed system is shown in Fig. 3. Considering most of the aforementioned challenging repetitive environments where the AMRs operate have flat/even surfaces [23], [24], this paper concentrates on the 3-DoF global localization problem, where the AMR pose $\mathbf{x}_t$ at time step $t \in \mathbb{Z}_{\geq 0}$ is a random variable which can be denoted as $\mathbf{x}_t = [x, y, \psi]^T \in \mathbb{R}^2 \times \mathbb{S}$, *i.e.*, the 2-D Euclidean space with corresponding orientation.

As aforementioned in Section II-A, commonly used MF-based localization algorithms suffer from the orientation-dependent characteristic of the 3-D MF vector [23], [33], [36] and the similar-sequential-route limitation [33], [36]. Therefore, we propose the probabilistic global localization framework with 2-D LiDAR and rotation-invariant MF to address the aforementioned problems. A novel sliding magnetometer mechanism is also designed and implemented to greatly improve the initialization robustness and accuracy.

Problem: *The problem of probabilistic global localization in repetitive and ambiguous environments can be formulated as the estimation of joint probabilistic distribution:*

$$p\left(\mathbf{x}_t, \mathbf{x}_0 | \mathbf{z}_0, \mathbf{z}_{1:t}, \mathbf{u}_{1:t}, \mathbb{M}\right) = p(\mathbf{x}_0|\mathbf{z}_0, \mathbb{M})\, p(\mathbf{x}_t|\mathbf{x}_0, \mathbf{z}_{1:t}, \mathbf{u}_{1:t}, \mathbb{M}^{\mathbb{B}}) \tag{3}$$

We assume the independence of each sensor observation. We denote the sensor observation as $\mathbf{z} = [\mathbf{z}_0, \mathbf{z}_{1:t}]^T$, where $\mathbf{z}_0 = [\mathbf{z}_0^L, \mathbf{z}_0^B]^T$ and $\mathbf{z}_{1:t}$ depict sensor observations of the two-step initialization submodule at timestep 0 and MF observations of the pose tracking submodule from time 1 to t, respectively. We denote the candidate initial poses as

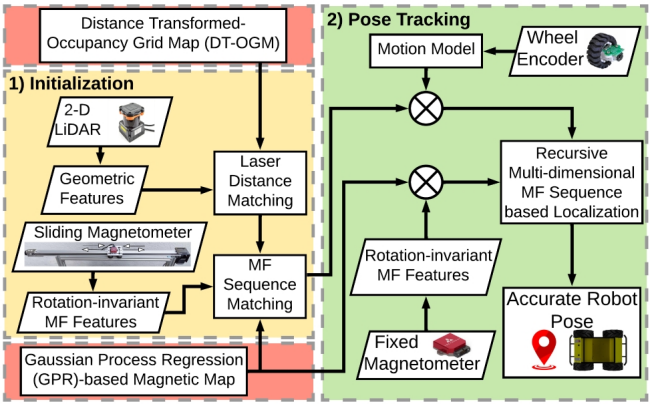

Fig. 3. Framework of the proposed probabilistic global localization system. The whole system can be divided into two submodules: a) *Two-step Initialization*; b) *Magnetic Field-based Pose Tracking*. The pre-built DT-OGM and GPR-based magnetic map are shown in red.

$\mathbf{x}_0 \in \{\langle \mathbf{x}_0^1, \mathbf{x}_0^2, ..., \mathbf{x}_0^i \rangle \,|\, i = 1, ..., N\}$, where N depicts the numbers of selected candidates. With respect to (*w.r.t.*) $\mathbf{x}_0$, we denote the fine pose as $\mathbf{x}_t \in \{\langle \mathbf{x}_t^1, \mathbf{x}_t^2, ..., \mathbf{x}_t^i \rangle \,|\, i = 1, ..., N\}$. $\mathbf{u}$ denotes the control input. Map $\mathbb{M} = [\mathbb{M}^{\mathbb{L}}, \mathbb{M}^{\mathbb{B}}]^T$ consists of the DT-OGM $\mathbb{M}^{\mathbb{L}}$ and magnetic map $\mathbb{M}^{\mathbb{B}}$.

A. *Two-step Initialization*

First, we analyze the initialization submodule $p(\mathbf{x}_0|\mathbf{z}_0, \mathbb{M})$ in Eq. (3). The aim of initialization is to estimate the candidate initial pose $\mathbf{x}_0$, where we apply the Bayesian theorem as:

$$\begin{aligned} p(\mathbf{x}_0|\mathbf{z}_0, \mathbb{M}) &= \eta_0\, p(\mathbf{x}_0)\, p(\mathbf{z}_0|\mathbf{x}_0, \mathbb{M}) \\ &= \eta_0\, p(\mathbf{x}_0)\, p(\mathbf{z}_0^L|\mathbf{x}_0, \mathbb{M}^{\mathbb{L}})\, p(\mathbf{z}_0^B|\mathbf{x}_0, \mathbb{M}^{\mathbb{B}}) \end{aligned} \tag{4}$$

where η_0 is a normalization constant and $p(\mathbf{x}_0)$ is the prior estimation. The observation model $p(\mathbf{z}_0|\mathbf{x}_0, \mathbb{M})$ can be splitted into two parts: the laser range observation model $p(\mathbf{z}_0^L|\mathbf{x}_0, \mathbb{M}^{\mathbb{L}})$ and the MF observation model $p(\mathbf{z}_0^B|\mathbf{x}_0, \mathbb{M}^{\mathbb{B}})$. We assume the prior distribution of each candidate pose $p(\mathbf{x}_0)$ to be a uniform distribution [38]. The laser range and MF observation models are detailed below, respectively.

1) Laser Range Observation Model: First, the candidate initial poses are selected based on the laser range information. The laser range observation model is built upon the transformed distance [39], where the distance transformed occupancy grid map (DT-OGM) is built in the offline phase. We select the candidate initial poses based on the constraint:

$$\delta(d_0^i) = |d_0^i - d_0^m| \leq d_{th} \tag{5}$$

where d_0^i denotes the transformed distance from the i-th candidate initial location to its closest obstacles in the DT-OGM and d_0^m is the actual minimum measured laser range to the closest obstacles. Considering the uncertainty of laser range scan, the transformed distance threshold is empirically set as $d_{th} = 0.05$. Based on the normal distribution [38], the observation model $p(\mathbf{z}_0^L|\mathbf{x}_0, \mathbb{M}^{\mathbb{L}})$ can be denoted as:

$$p(\mathbf{z}_0^L|\mathbf{x}_0,\mathbb{M}^{\mathbb{L}}) \propto \prod_{i=1}^{N} \frac{1}{\sigma\sqrt{2\pi}} \exp\Big(-\frac{1}{2}\frac{\big(d_0^i - d_0^m\big)^2}{\sigma^2}\Big) \quad (6)$$

where σ denotes the standard deviation of the laser range measurements. Multiple candidates are retained due to the similarities of the transformed distance.

2) MF Observation Model: After the initialization by laser-based transformed distance, the MF sequence measured by the designed sliding magnetometer mechanism with corresponding local coordinates are matched with the magnetic map to further eliminate the false positive candidates. Considering at timestep 0, the online measured MF sequence with rotation-invariant MF vectors can be denoted as $\mathbf{B_O^0} = \{\mathbf{B}_{O,1}^0, \mathbf{B}_{O,2}^0, ..., \mathbf{B}_{O,k}^0\}$, where $\mathbf{B}_{O,k}^0 = [B_{O,k}^{h,0}, B_{O,k}^{v,0}, F_{O,k}^0]^T$. Then, we denote the observation function as $obv(\mathbf{x}_0^i)$ to return the MF sequence in the magnetic map that is geographically closest to the AMR candidate initial pose $\mathbf{x}_0^i$. For the convenience of describing the problem, we define the $\mathcal{R} = \{\{\mathbf{r}_{i,k}\}_{i=1}^N\}_{k=1}^K$ as the residual, where $\mathbf{r}_{i,k} = \mathbf{B}_{O,k}^0 - obv(\mathbf{x}_0^{i,k})$. Therefore, the MF observation model can be denoted by applying the k-dimensional Gaussian pseudo distribution as [1], [28]:

$$p(\mathbf{z}_0^B|\mathbf{x}_0,\mathbb{M}^{\mathbb{B}}) \propto \prod_{i=1}^{N}\prod_{k=1}^{K} \frac{1}{(2\pi)^{\frac{k}{2}}|\mathbf{C}_{i,k}|^{\frac{1}{2}}} \cdot \exp\big(-\frac{1}{2}\mathbf{r}_{i,k}^T\mathbf{C}_{i,k}^{-1}\mathbf{r}_{i,k}\big) \quad (7)$$

where the covariance matrix of $\mathbf{r}_{i,k}$ is defined as $\mathbf{C}_{i,k} \triangleq \Sigma_{\mathbf{B}_O^0}^k + \mathbf{R}\Sigma_{\mathbf{x}_0^i}^k\mathbf{R}^{\mathbf{T}}$. $\Sigma_{\mathbf{B}_O^0}^k$ and $\Sigma_{\mathbf{x}_0^i}^k$ are the covariance matrix of the two MF vectors, respectively, while $\mathbf{R}$ is the rotation matrix. After the aforementioned two initialization steps, a number of N candidate initial poses are selected and sent as input for the subsequent *MF-based pose tracking* submodule.

B. Magnetic Field-based Pose Tracking

We move forward to analyze the pose tracking term in Eq. (3). The objective of pose tracking is to infer and track the accurate AMR pose $\mathbf{x}_t$, where we apply the Bayesian theorem and Markov property, and derivate it as:

$$\begin{aligned} &p(\mathbf{x}_t|\mathbf{x}_0,\mathbf{z}_{1:t},\mathbf{u}_{1:t},\mathbb{M}^{\mathbb{B}}) \\ &= \eta_t\, p(\mathbf{z}_t|\mathbf{x}_t,\mathbf{x}_0,\mathbf{z}_{1:t-1},\mathbf{u}_{1:t},\mathbb{M}^{\mathbb{B}})\, p(\mathbf{x}_t|\mathbf{x}_0,\mathbf{z}_{1:t-1},\mathbf{u}_{1:t},\mathbb{M}^{\mathbb{B}}) \\ &= \eta_t\, p(\mathbf{z}_t|\mathbf{x}_t,\mathbb{M}^{\mathbb{B}})\, p(\mathbf{x}_t|\mathbf{x}_0,\mathbf{u}_{1:t}) \end{aligned} \quad (8)$$

where η_t is also a normalization constant. $p(\mathbf{z}_t|\mathbf{x}_t,\mathbb{M}^{\mathbb{B}})$ and $p(\mathbf{x}_t|\mathbf{x}_0,\mathbf{u}_{1:t})$ are the observation model and motion model of the pose tracking submodule, respectively. A standard odometry motion model is employed for the AMR, where we refer the details to [38]. For the observation model, it can be derivated with recursive multi-dimensional MF sequence matching, where the details are presented below.

To address the aforementioned similar-sequential-route problem [33], [36], we propose a novel recursive multi-dimensional MF sequence matching method to align two time series MF sequences. In general, considering two MF sequences from timestep $t-n$ to t (*i.e.*, $n+1$ dimension): the online measured MF sequence with local coordinates as $\mathbf{B_O} = \{\mathbf{B}_O^{t-n}, \mathbf{B}_O^{t-n+1}, ..., \mathbf{B}_O^t\}$, where $\mathbf{B}_O^t = [B_O^{h,t}, B_O^{v,t}, F_O^t]^T$ denotes the rotation-invariant 3-D MF vector measured at time t; and the motion model based MF sequence with global coordinates in the magnetic map *w.r.t.* the i-th candidate location as $\mathbf{B_{M}}^i = \{\mathbf{B}_{M^i}^{t-n}, \mathbf{B}_{M^i}^{t-n+1}, ..., \mathbf{B}_{M^i}^t\}$, where $\mathbf{B}_{M^i}^t = [B_{M^i}^{h,t}, B_{M^i}^{v,t}, F_{M^i}^t]^T$. Thereafter, the observation model of the pose tracking submodule can be derivated based on the multivariate multi-dimensional Gaussian distribution as:

$$p(\mathbf{z}_t|\mathbf{x}_t,\mathbb{M}^{\mathbb{B}}) \propto \prod_{i=1}^{N} \frac{\exp\Big(-\frac{1}{2}(\mathbf{B_O}-\mathbf{B_M}^i)^T\mathbf{\Sigma}_{\mathbf{x}_t^i}^{-1}(\mathbf{B_O}-\mathbf{B_M}^i)\Big)}{(\sqrt{2\pi})^{n+1}\sqrt{|\mathbf{\Sigma}_{\mathbf{x}_t^i}|}} \quad (9)$$

where $\mathbf{\Sigma}_{\mathbf{x}_t^i} = \{\Sigma_{\mathbf{x}_t^i}^{t-n}, \Sigma_{\mathbf{x}_t^i}^{t-n+1}, ..., \Sigma_{\mathbf{x}_t^i}^t\}$ is the sequence of diagonal covariance matrix of the MF measurements at the i-th candidate location, while the diagonal elements of the covariance matrix $\Sigma_{\mathbf{x}_t^i}^t$ at time t can be shown as $\sigma_{\mathbf{x}_t^i}^{h,t}$, $\sigma_{\mathbf{x}_t^i}^{v,t}$, and $\sigma_{\mathbf{x}_t^i}^{F,t}$. When the AMR moves forward, the MF vector at timestep $t-n$ will be discarded and the upcoming MF vector at timestep $t+1$ will be included in the MF sequence, thus making this a recursive and continuous localization process.

After the aforementioned process, we empirically select a number of Q candidates with low matching errors. Eventually by integrating the initialization (Eq. (4)) and pose tracking (Eq. (8)) submodules, the accurate AMR pose $\mathbf{x}_t$ defined in Eq. (3) can be inferred by the Q selected candidates as:

$$\varepsilon[\mathbf{x}_t] = \frac{\sum_{i=1}^{Q}\Big(\mathbf{x}_t^i \cdot p(\mathbf{x}_0^i|\mathbf{z}_0,\mathbb{M}) \cdot p(\mathbf{x}_t^i|\mathbf{x}_0^i,\mathbf{z}_{1:t},\mathbf{u}_{1:t},\mathbb{M}^{\mathbb{B}})\Big)}{\sum_{i=1}^{Q}\Big(p(\mathbf{x}_0^i|\mathbf{z}_0,\mathbb{M}) \cdot p(\mathbf{x}_t^i|\mathbf{x}_0^i,\mathbf{z}_{1:t},\mathbf{u}_{1:t},\mathbb{M}^{\mathbb{B}})\Big)} \quad (10)$$

IV. Experimental Validations and Discussions

A. Simulations and Experiments Setup

The simulated and real AMR platform used are shown in Fig. 4. One Hokuyo UTM-30LX 2-D LiDAR is installed in front and one VN-100T IMU/magnetometer is mounted at the top frame with the designed sliding mechanism. After the two-step initialization phase, the magnetometer is fixed

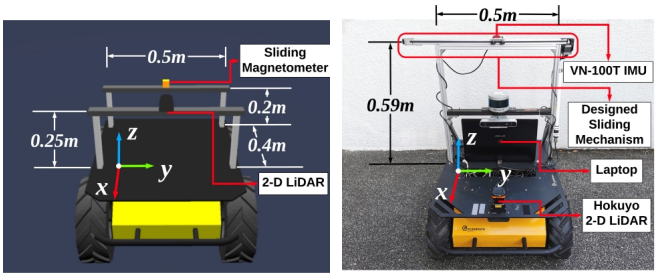

(a) Simulated AMR platform (b) Real AMR platform

Fig. 4. *Clearpath Husky A200* AMR platform and body frame. We self-designed the sensor suite and calibrated all the sensors before experiments. To avoid possible MF distortions from other sensors, the IMU installed at the sliding mechanism is 0.59m higher than the real AMR platform.

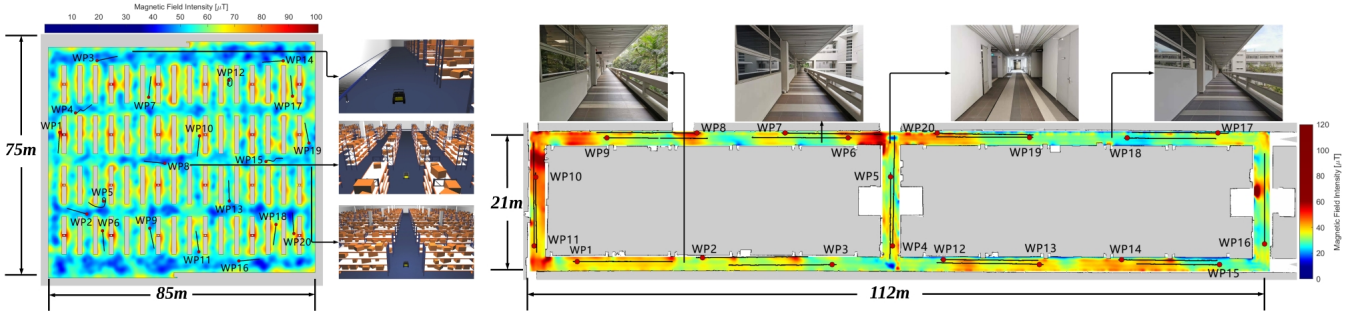

(a) Simulated Industrial Warehouse

(b) Real Office Corridor

Fig. 5. (a) and (b) visualize the fused GPR-based magnetic maps and OGMs of the simulated industrial warehouse and real office corridor environments, respectively. Within each fused map, the color depicts the MF integrated intensity based on the colorbar. Red dots denote randomly-selected waypoints (WPs, *i.e.,* global localization starting locations) and black lines denote the ground-truth trajectories of the AMR.

at the center point of the sliding bar throughout the pose tracking phase. All the experiments are executed on a laptop with an Intel i7-10875H CPU @2.3GHz with 32GB RAM.

Experimental Environment: We conducted experiments in one simulated indoor industrial warehouse and one real office corridor environment, which are:

a) Simulated industrial warehouse: As shown in Fig. 5a, the warehouse size is $85m \times 75m$, and consists of repetitive goods shelves, steel concrete pillars, and conveyor belts. The rotation-invariant 3-D MF fingerprints collected in an open space area around the same size serves as the basis. Then, local MF variations such as steel concrete pillars and steel goods shelves were modeled according to [26], [40], and they were overlaid on the basic MF data. The lateral distance between the data collection routes is empirically set at $0.6m$ to balance between the mapping accuracy and efficiency.

b) Real long corridor: As shown in Fig. 5b, the corridor size is $112m \times 21m$, and consists of repetitive straight fences and symmetric walls. The lateral distance between the data collection routes is empirically set at $0.5m$.

OGM / DT-OGM Building: 2-D SLAM algorithm *Gmapping* of the ROS package was implemented to build the 2-D occupancy grid maps (OGMs). High percentage of these OGMs are distorted or failed because of the repetitive configurations [2], where we choose to use the most accurate OGM among all the OGMs that we built. Then, the *distanceTransform* function in the OpenCV library is called to build the corresponding DT-OGM.

Magnetic Map Building: With the acquired ground-truth initial pose, we manually operated the AMR while implementing LiDAR-based PF algorithm [41] in the pre-built OGM to estimate the magnetometer locations [27].

To improve the efficiency of MF data collection, the AMR was manually operated to follow different designated trajectories to cover as much traversable area of the warehouse and corridor as possible. For the two environments, the number of collected MF fingerprints were 192,723 and 83,103, respectively. Similarly with our previous work [23], the collected rotation-invariant MF fingerprints are then utilized to build the Gaussian Process Regression (GPR)-based magnetic map since it is the most accurate. Eventually, the GPR-based magnetic maps fused with the OGMs of the two environments are shown in Fig. 5 as illustrations.

B. Evaluation Protocol

1) ***Comparison Baseline****:* As far as we know, no publicly available work is focused on the MF and LiDAR fusion based global localization. Thus, we present detailed quantitative analysis of our proposed localization system comparing with six different MF-based global localization algorithms, which are: 1) *MSTSL* [23]: our previous two-step localization method; 2) *k-NN* [34]: the well-known *k*-NN classification method; 3) *LocateMe* [26]: the original dynamic time warping (DTW) algorithm with 1-D MF magnitude; 4) *MagSequence* [36]: the DTW algorithm with 3-D MF vectors; 5) *1-D PF* [1]: particle filtering (PF)-based 1-D MF magnitude localization; 6) *3-D PF* [30]: PF-based 3-D MF vector localization. We randomly selected twenty waypoints (WPs) in each environment to do the evaluation. The ground-truth locations of these WPs and trajectories were obtained by combining the initial position manually measured by a tape ruler with the 3-D SLAM odometry acquired from LeGo-LOAM [42]. For each evaluated approach of each WP, ten individual random tests were conducted.

2) ***Evaluation Metrics****:* For the evaluation of AMR global localization performance of each comparative method, we implement three criterions, which are: 1) Convergence; 2) Accuracy; and 3) Efficiency. First, we assess the convergence of global localization by the Convergence Rate (*CR*), which denotes the ratio of the number of frames with high accuracy over the total number of localization frames. We empirically define a threshold of $3.0m$ for the mean squared of the translational error (*MSE*) to determine whether each single frame in each WP is successful/converged ($MSE \leq 3.0m$) or failed ($MSE > 3.0m$). Besides, we utilize the Cumulative Distribution Function (*CDF*) of the *MSE* to evaluate the tracking accuracy of the AMR. Moreover, we assess the localization efficiency by measuring the actual computational time of each method to successfully localize the AMR within the *MSE* threshold of $3.0m$.

C. Experimental Evaluations

The performance comparisons of the proposed localization system with the aforementioned six global localization methods are analyzed in this subsection.

1) Localization Convergence: In Fig. 6a and Fig. 6d, the localization convergence assessed by *CR* is illustrated as

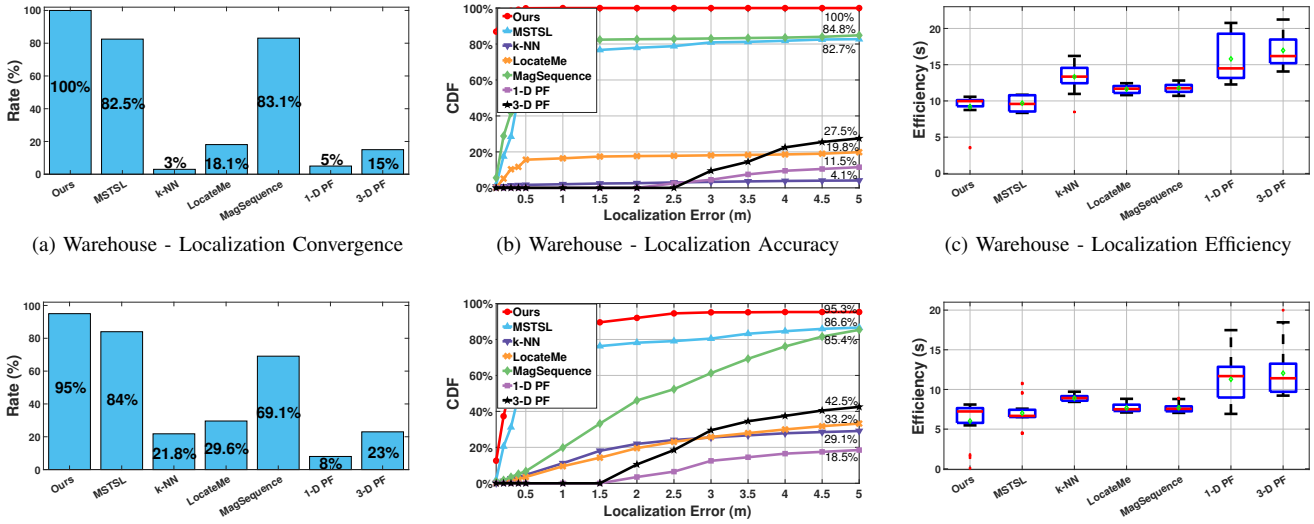

(a) Warehouse - Localization Convergence (b) Warehouse - Localization Accuracy (c) Warehouse - Localization Efficiency

(d) Corridor - Localization Convergence (e) Corridor - Localization Accuracy (f) Corridor - Localization Efficiency

Fig. 6. **Left**: (a) and (d) are the histograms illustrating the global localization convergence rate (*CR*). **Middle**: (b) and (e) demonstrate the *CDF* plots of the overall global localization error. **Right**: (c) and (f) demonstrate boxplots summarization of the computational time over each waypoint of each environment. The green diamond, horizontal red line, and red cross mark denote the mean value, median value, and the outlier, respectively.

histograms. In both environments, the proposed localization system achieves the highest *CR* of **100**% and of **95**%, respectively, while the *CRs* of the comparative methods is varying from 3% to 84%. The only failure case of our proposed method is in WP#5 of the corridor environment, which is very close to the elevator with strong magnetic distortions, thus causing the AMR to be mis-localized. Besides, it is easy to tell that the aforementioned similar-sequential-route limitation has greatly deteriorated the performances of *LocateMe* and *MagSequence*, as four of the localization routes are curved (WP#4, WP#5, WP#12, and WP#15) as shown in Fig. 5a.

2) Localization Accuracy: Fig. 6b and Fig. 6e demonstrate the localization accuracy. For the *MSE* that is within $1.5m$, the proposed localization method yields a more than 90 percentile *CDF*. Besides, *MagSequence* has comparative performances with the *MSTSL* method, and both of them closely follows the trend of the proposed localization method but outperforms the other comparative methods by a large margin. Moreover, the accuracy of simple classification method *k*-NN is significantly degraded in such challenging scenarios and is not able to accomplish the localization tasks. From these results, it is evident that the proposed method significantly outperforms the *MSTSL* and PF-based methods.

3) Localization Efficiency: The localization efficiency is summarized in Fig. 6c and Fig. 6f. It is clear that the proposed localization method costs the least amount of computational time whether *w.r.t.* the mean value or the median value, thus indicating the superior computational efficiency. The proposed method takes less than $9.2s$ and $6s$ on average to successfully localize the AMR in these two environments, respectively. As comparison, the average time which the comparative methods cost varies from $9.6s$ to $17s$ and from $7s$ to $12s$ in these two environments, respectively.

V. Conclusion

This paper presented a novel probabilistic global localization system with 2-D LiDAR and rotation-invariant magnetic field (MF) for autonomous mobile robots (AMRs) operating in repetitive and ambiguous environments, which solves both the orientation-dependency and similar-sequential-route limitations of previous MF-based localization methods. The proposed localization system comprises the laser distance and MF sequence matching based two-step initialization, and recursive multi-dimensional MF sequence based pose tracking. The extensive experimental results have presented the capability of the proposed system to robustly localize the AMR in challenging repetitive environments, demonstrating the advantageous accuracy and efficiency of the proposed system over the comparative methods. In the future, fusions of our system with 3-D laser/vision-based methods can be performed to further improve the localization robustness.

References

[1] J. Haverinen and A. Kemppainen, "Global indoor self-localization based on the ambient magnetic field," *Robot. Auton. Syst.*, vol. 57, no. 10, pp. 1028–1035, 2009.

[2] Z. Wu *et al.*, "Infrastructure-free global localization in repetitive environments: An overview," in *Proc. IECON 2020 - 46th Annu. Conf. of the IEEE Ind. Electron. Soc.* IEEE, 2020, pp. 626–631.

[3] Z. Wang, L. Zhang, S. Zhao, and S. Zhang, "Global localization with a single-line LiDAR by dense 2D signature and 1D registration," *IEEE Sens. J.*, vol. 21, no. 10, pp. 11 497–11 506, 2020.

[4] X. Chen, T. Läbe, L. Nardi, J. Behley, and C. Stachniss, "Learning an overlap-based observation model for 3D LiDAR localization," in *Proc. IEEE/RSJ Int. Conf. Intell. Robots Syst. (IROS)*. IEEE, 2020, pp. 4602–4608.

[5] Y. Wang, M. Shan, Y. Yue, and D. Wang, "Autonomous target docking of nonholonomic mobile robots using relative pose measurements," *IEEE Trans. Ind. Electron. (TIE)*, vol. 68, no. 8, pp. 7233–7243, 2020.

[6] Z. Wu, Y. Yue, M. Wen, J. Zhang, J. Yi, and D. Wang, "Infrastructure-free hierarchical mobile robot global localization in repetitive environments," *IEEE Trans. Instrum. Meas. (TIM)*, vol. 70, pp. 1–12, 2021.

[7] X. Chen, I. Vizzo, T. Läbe, J. Behley, and C. Stachniss, "Range image-based lidar localization for autonomous vehicles," in *Proc. IEEE Int. Conf. Robot. Autom. (ICRA)*. IEEE, 2021, pp. 5802–5808.

[8] Q. Zhang, M. Wang, Y. Yue, and T. Liu, "LCR-SMM: Large convergence region semantic map matching through expectation maximization," *IEEE/ASME Trans. Mechatron. (TMECH)*, vol. 27, no. 5, pp. 3029–3040, 2021.

[9] Y. Wang, Q. Liu, E. Mihankhah, C. Lv, and D. Wang, "Detection and isolation of sensor attacks for autonomous vehicles: Framework, algorithms, and validation," *IEEE Trans. Intell. Transp. Syst. (TITS)*, vol. 23, no. 7, pp. 8247–8259, 2021.

[10] D. Su, H. Kong, S. Sukkarieh, and S. Huang, "Necessary and sufficient conditions for observability of SLAM-based TDOA sensor array calibration and source localization," *IEEE Trans. Robot. (TRO)*, vol. 37, no. 5, pp. 1451–1468, 2021.

[11] H. Dong, X. Chen, S. Särkkä, and C. Stachniss, "Online pole segmentation on range images for long-term lidar localization in urban environments," *Robot. Auton. Syst.*, vol. 159, p. 104283, 2023.

[12] Y. Yue *et al.*, "Day and night collaborative dynamic mapping in unstructured environment based on multimodal sensors," in *Proc. IEEE Int. Conf. Robot. Autom. (ICRA)*. IEEE, 2020, pp. 2981–2987.

[13] Y. Yue, C. Zhao, M. Wen, Z. Wu, and D. Wang, "Collaborative semantic perception and relative localization based on map matching," in *Proc. IEEE/RSJ Int. Conf. Intell. Robots Syst. (IROS)*. IEEE, 2020, pp. 6188–6193.

[14] Y. Yue, C. Zhao, Z. Wu, C. Yang, Y. Wang, and D. Wang, "Collaborative semantic understanding and mapping framework for autonomous systems," *IEEE/ASME Trans. Mechatron. (TMECH)*, vol. 26, no. 2, pp. 978–989, 2020.

[15] G. Peng, Y. Yue, J. Zhang, Z. Wu, X. Tang, and D. Wang, "Semantic reinforced attention learning for visual place recognition," in *Proc. IEEE Int. Conf. Robot. Autom. (ICRA)*. IEEE, 2021, pp. 13 415–13 422.

[16] G. Peng, J. Zhang, H. Li, and D. Wang, "Attentional pyramid pooling of salient visual residuals for place recognition," in *Proc. IEEE/CVF Int. Conf. Comput. Vis. (ICCV)*, 2021, pp. 885–894.

[17] S. Jin, Z. Wu, C. Zhao, J. Zhang, G. Peng, and D. Wang, "SectionKey: 3-D semantic point cloud descriptor for place recognition," in *Proc. IEEE/RSJ Int. Conf. Intell. Robots Syst. (IROS)*. IEEE, 2022, pp. 9905–9910.

[18] G. Peng, Y. Huang, H. Li, Z. Wu, and D. Wang, "LSDNet: A lightweight self-attentional distillation network for visual place recognition," in *Proc. IEEE/RSJ Int. Conf. Intell. Robots Syst. (IROS)*. IEEE, 2022, pp. 6608–6613.

[19] A. Abosekeen, A. Noureldin, and M. J. Korenberg, "Improving the RISS/GNSS land-vehicles integrated navigation system using magnetic azimuth updates," *IEEE Trans. Intell. Transp. Syst. (TITS)*, vol. 21, no. 3, pp. 1250–1263, 2019.

[20] S. Eiffert, N. D. Wallace, H. Kong, N. Pirmarzdashti, and S. Sukkarieh, "Resource and response aware path planning for long-term autonomy of ground robots in agriculture," *Field Robotics*, vol. 2, pp. 1–33, 2022.

[21] Y. Wang, X. Liu, Y. Kang, and S. S. Ge, "Anomaly resilient relative pose estimation for multiple nonholonomic mobile robot systems," *IEEE Sens. J.*, vol. 16, no. 1, pp. 659–670, 2020.

[22] Y. Yue and D. Wang, *Collaborative Perception, Localization and Mapping for Autonomous Systems*. Springer Nature, 2020, vol. 2.

[23] Z. Wu, Y. Yue, M. Wen, J. Zhang, G. Peng, and D. Wang, "MSTSL: Multi-sensor based two-step localization in geometrically symmetric environments," in *Proc. IEEE Int. Conf. Robot. Autom. (ICRA)*. IEEE, 2021, pp. 5245–5251.

[24] M. G. Puyol, D. Bobkov, P. Robertson, and T. Jost, "Pedestrian simultaneous localization and mapping in multistory buildings using inertial sensors," *IEEE Trans. Intell. Transp. Syst. (TITS)*, vol. 15, no. 4, pp. 1714–1727, 2014.

[25] B. Li, T. Gallagher, A. G. Dempster, and C. Rizos, "How feasible is the use of magnetic field alone for indoor positioning?" in *Proc. Int. Conf. Ind. Posi. Ind. Navi. (IPIN)*. IEEE, 2012, pp. 1–9.

[26] K. P. Subbu, B. Gozick, and R. Dantu, "LocateMe: Magnetic-fields-based indoor localization using smartphones," *ACM Trans. Intell. Syst. and Tech.*, vol. 4, no. 4, pp. 1–27, 2013.

[27] N. Akai and K. Ozaki, "Gaussian processes for magnetic map-based localization in large-scale indoor environments," in *Proc. IEEE/RSJ Int. Conf. Intell. Robots Syst. (IROS)*, 2015, pp. 4459–4464.

[28] H. Xie, T. Gu, X. Tao, H. Ye, and J. Lu, "A reliability-augmented particle filter for magnetic fingerprinting based indoor localization on smartphone," *IEEE Trans. Mobile Comput.*, vol. 15, no. 8, pp. 1877–1892, 2015.

[29] Z. Wu, M. Wen, G. Peng, X. Tang, and D. Wang, "Magnetic-assisted initialization for infrastructure-free mobile robot localization," in *Proc. 2019 IEEE Int. Conf. on Cyb. and Intelli. Syst. (CIS) and IEEE Conf. on Robot., Autom. and Mechatron. (RAM)*. IEEE, 2019, pp. 518–523.

[30] M. Frassl, M. Angermann, M. Lichtenstern, P. Robertson, B. J. Julian, and D. Marek, "Magnetic maps of indoor environments for precise localization of legged and non-legged locomotion," in *Proc. IEEE/RSJ Int. Conf. Intell. Robots Syst. (IROS)*, 2013, pp. 913–920.

[31] J. Jung, S.-M. Lee, and H. Myung, "Indoor mobile robot localization and mapping based on ambient magnetic fields and aiding radio sources," *IEEE Trans. Instrum. Meas. (TIM)*, vol. 64, no. 7, pp. 1922–1934, 2015.

[32] Y. Shu, C. Bo, G. Shen, C. Zhao, L. Li, and F. Zhao, "Magicol: Indoor localization using pervasive magnetic field and opportunistic WiFi sensing," *IEEE J. Sel. Areas Commun.*, vol. 33, no. 7, pp. 1443–1457, 2015.

[33] S. Wang, H. Wen, R. Clark, and N. Trigoni, "Keyframe based large-scale indoor localisation using geomagnetic field and motion pattern," in *Proc. IEEE/RSJ Int. Conf. Intell. Robots Syst. (IROS)*. IEEE, 2016, pp. 1910–1917.

[34] S.-C. Yeh *et al.*, "Study on an indoor positioning system using Earth's magnetic field," *IEEE Transactions on Instrumentation and Measurement*, vol. 69, no. 3, pp. 865–872, 2019.

[35] Y. Shu, K. G. Shin, T. He, and J. Chen, "Last-mile navigation using smartphones," in *Proc. 21st Annu. Int. Conf. Mobile Comput. Netw. (MobiCom)*, 2015, pp. 512–524.

[36] C. Gao and R. Harle, "Sequence-based magnetic loop closures for automated signal surveying," in *Proc. Int. Conf. Ind. Posi. Ind. Navi. (IPIN)*. IEEE, 2015, pp. 1–12.

[37] VectorNav Technologies. "VN-100 user manual" Accessed on: Apr. 12, 2022. [Online]. Available: https://www.vectornav.com/resources/user-manuals/vn-100-user-manual

[38] S. Thrun, W. Burgard, and D. Fox, *Probabilistic robotics*. The MIT press, 2005.

[39] P. F. Felzenszwalb and D. P. Huttenlocher, "Distance transforms of sampled functions," *Theory of Computing*, vol. 8, no. 1, pp. 415–428, 2012.

[40] E. Čermáková, "Magnetization of steel building materials and structures in the natural geomagnetic field," *Acta Polytechnica*, vol. 45, no. 6, 2005.

[41] S. Thrun, D. Fox, W. Burgard, and F. Dellaert, "Robust monte carlo localization for mobile robots," *Arti. Intelli.*, vol. 128, no. 1-2, pp. 99–141, 2001.

[42] T. Shan and B. Englot, "LeGo-LOAM: Lightweight and ground-optimized lidar odometry and mapping on variable terrain," in *Proc. IEEE/RSJ Int. Conf. Intell. Robots Syst. (IROS)*. IEEE, 2018, pp. 4758–4765.